PHYSICAL REVIEW C VOLUME 24, NUMBER 5 NOVEMBER 1981

Photon scattering studies of the giant dipole resonance in medium weight nuclei

T. J. Bowles,[1]* R. J. Holt,[1] H. E. Jackson,[1] R. M. Laszewski,[2]
R. D. McKeown,[1]† A. M. Nathan,[2] and J. R. Specht[1]
[1]*Argonne National Laboratory, Argonne, Illinois 60439*
[2]*University of Illinois at Urbana-Champaign, Urbana, Illinois 61801*
(Received 26 May 1981)

Quasimonochromatic photons have been used to measure elastic and inelastic photon scattering cross sections in the giant dipole resonance region of ^{52}Cr, Fe, ^{60}Ni, ^{92}Mo, and ^{96}Mo in an experiment in which the elastic and inelastic scattering are resolved. The elastic scattering cross sections show clear evidence for isospin splitting of the giant dipole resonance. The inelastic scattering to low-lying vibrational levels, which is a measure of the coupling between the giant dipole resonance and collective surface vibrations, is in qualitative agreement with the predictions of the dynamic collective model. However, when examined in detail, this model does not provide an adequate description of the scattering data.

[NUCLEAR REACTIONS ^{52}Cr, Fe, ^{60}Ni, ^{92,96}Mo (γ,γ'), $14 \leq E_\gamma \leq 22$ MeV; measured E_γ, $E_{\gamma'}$, $d\sigma/d\Omega$ for γ_0,γ_1. Compared to DCM predictions. Tagged photons.]

I. INTRODUCTION

The giant dipole resonance (GDR) is one of the simplest and most basic features of nuclear matter. It was discovered in the earliest days of nuclear physics and has since been studied in great detail. While we know many of its features with great precision, some of the properties associated with its decay are less well understood. There has been considerable experimental activity in recent years devoted to measurements of the decay branches of giant resonances. Nevertheless, it has been known for many years that in medium and heavy nuclei, the GDR decay is largely dominated by the statistical evaporation of neutrons.[1] Thus, for $A \gtrsim 40$, by the time the GDR decays, it has evolved from a coherent vibration into the complicated motion of the compound nucleus. If this picture is accurate, one can legitimately ask whether the study of the decays of giant resonances will teach us anything about their basic structure or about how they couple to more complicated modes.

One possible exception is the photon decay mode, which is best studied with the photon-scattering reaction. The elastic-scattering process is clearly nonstatistical since a collective mode that is excited by absorption of a photon can collectively deexcite to the ground state by reemission of a photon. In fact, elastic scattering cross sections are constrained by the photoabsorption cross section via the optical theorem and a dispersion relation.[2] However, it is less well appreciated that photon decays to low-lying excited states, which are measured via inelastic photon scattering, may also be nonstatistical, even in nuclei where the particle decays of the GDR are largely statistical. These inelastic branches arise from the coupling of the basic dipole oscillation to low-lying collective degrees of freedom, such as quadrupole surface vibrations. Elementary considerations lead one to expect a strong coupling between dipole and quadrupole modes,[3] resulting both in a broadening of the resonance shape observed in total photoabsorption cross sections[4] and in a substantial branching ratio of photon decay to low-lying excited states.[5] In fact, photon scattering is an ideal reaction for probing the coupling of the various modes of nuclear motion since inelastic scattering to low-lying vibrational states provides a direct measure of the strength of vibrational components in the wave function of the giant dipole state.[5]

In this paper we test the predictions of the

Dynamic Collective Model (DCM),[6] which attempts to describe the effects of dipole-quadrupole coupling on the photon-decay branches of the GDR. We present the results of photon scattering by the GDR in the group of medium-weight nuclei ^{52}Cr, Fe, ^{60}Ni, ^{92}Mo, and ^{96}Mo. The characteristics of the low-lying collective states in these nuclei are varied enough to allow a meaningful investigation of the systematics of dipole-quadrupole coupling. The experiments emphasize the observation of inelastic scattering to excited vibrational states using beams of quasimonochromatic incident photons and a detector in which the elastic and inelastic photon scattering are resolved. The elastic scattering data show clear evidence for the isospin splitting of the GDR,[7] while the inelastic scattering data show a substantial nonstatistical cross section which is in qualitative agreement with the predictions of the DCM. However, when examined in detail the DCM will be shown to provide an inadequate description of the scattering data.

In Sec. II we present a description of the experimental technique and data reduction. In Sec. III the data are analyzed in the framework of the DCM and this analysis forms the basis for the discussion of Sec. IV. Our conclusions are summarized in Sec. V. Preliminary accounts of this research have appeared elsewhere.[8,9]

II. EXPERIMENTAL METHOD

In order to observe directly inelastic photon scattering in the GDR region, it is essential that the combined energy resolution of the incident photon beam and the photon detector be sufficient to distinguish the inelastic from the elastic scattering. Until recently, attempts to perform these experiments have been hampered by the lack of intense monochromatic photon beams.[10–13] Two developments have made new measurements possible. These are, first, the availability of monochromatic photons from the University of Illinois tagged photon facility,[14] and second the fabrication of large-volume, high resolution NaI spectrometers that allow the resolution of elastic and inelastic photon scattering. The present experimental setup is shown schematically in Fig. 1. An electron beam from the MUSL-2 microtron strikes a 13.7 mg/cm^2 Al radiator (0.001 radiation lengths), thereby creating bremsstrahlung. Post-bremsstrahlung electrons are momentum-analyzed in a magnetic spectrometer and detected in coincidence with photons scattered from the target,

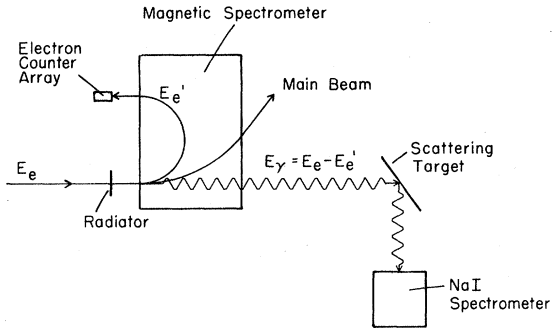

FIG. 1. Schematic diagram of the experimental arrangement.

thereby tagging the incident photon. The focal plane of the spectrometer contains 12 plastic scintillation counters which subdivide a 2.4-MeV segment of the bremsstrahlung spectrum into 12 contiguous 0.2-MeV segments.

The scattered photons were detected in a large NaI spectrometer, which is shown schematically in Fig. 2. The central element was a 24-cm diameter by 30-cm deep NaI(Tl) crystal viewed by seven RCA 4524 photomultiplier tubes. The detector was nearly completely surrounded by a neutron shield of ^{6}LiH and by an anticoincidence shield of NE102 plastic scintillator. Standard pulse-processing electronics were used.[15] For each NaI pulse above $\sim$10 MeV, an 8-nsec wide signal in timed coincidence with the 12 electron counters was used to strobe each of 12 coincidence circuits. These circuits were strobed a second time ($\sim$200 nsec later) in order to test for accidental coincidences. Thus, for each of the 12 electron counters, the corresponding γ-ray signal was routed into one of four 64-channel arrays, according to

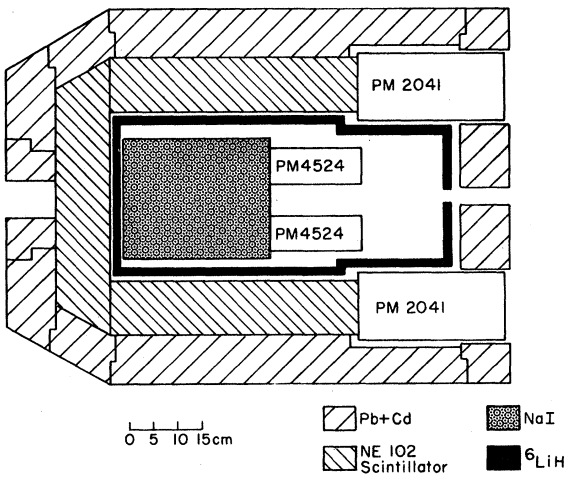

FIG. 2. Scale drawing of the NaI(Tl) spectrometer.

whether the coincidence was true or accidental and whether or not the NaI pulse was in coincidence with a signal from the anticoincidence plastic ("rejected" and "accepted", respectively). Under the typical experimental conditions described below, approximately 40% of the NaI pulses were "rejected" and the true-to-accidental coincidence ratio was ~ 10. For all the experiments, an overall energy resolution of 4% full width at half maximum (FWHM) or better was achieved in the NaI spectrometer.

At the start of each experiment, the NaI was put directly into a photon beam of greatly reduced intensity. This served three purposes. First, it allowed a quick diagnostic on the coincidence timing between the NaI and electron counters. Next, it allowed the accumulation of spectra representing the response of the NaI to essentially monochromatic photon beams for use in the subsequent data analysis. And finally, it directly measured the product of detector efficiency and photon flux for use in obtaining absolute cross sections, as described below.

For the scattering experiments, the detector was placed at an angle of 90° with respect to the incident photon beam, except for the case of ^{60}Ni for which it was at 120°. The solid angle (~ 117 msr) was defined by an aperture in a Pb collimator which excluded the edges of the NaI from direct illumination. The detector was shielded by at least 10 cm of Cd-loaded Pb so that only photons scattered from the target could reach the NaI. For most of the experiments, the electron beam was limited to a few nA, which resulted in counting rates of 30 kHz above 1 MeV in the NaI and 500 kHz above a 100-keV threshold in the anticoincidence shield. Each electron counter had a singles rate of about 1 MHz, corresponding to a *tagged* photon intensity of $\sim 4\times 10^5$ sec^{-1} on target for each 0.2-MeV bin. All of the targets used in the present studies were metallic samples, except for the ^{52}Cr which was in the form $^{52}Cr_2O_3$, and all except the Fe were enclosed in a thin-walled lucite container. Typical target thicknesses were 2–4 g/cm^2. The background was measured by replacing the sample with an empty container. In order to determine the background for the $^{52}Cr_2O_3$ sample, the lucite container was filled with water. A separate experiment was performed with graphite and polyethylene targets in order to calibrate the measurements against the well-known 15.11-MeV resonance[16] in ^{12}C. Most of the data were collected in 3 overlapping steps of $E_\gamma = 15.92-18.28$ MeV, $E_\gamma = 17.92-20.27$ MeV, and $E_\gamma = 19.87-22.22$ MeV. For ^{96}Mo data were also taken for $E_\gamma = 14.14-16.53$ MeV, and for Fe, data were repeated for $E_\gamma = 17.79-20.18$ MeV. The ^{60}Ni experiment was performed separately from the others in three steps from 14.75 to 21.40 MeV, as reported earlier.[8] The measured cross sections in the various regions of overlap were in good agreement in all cases.

Figure 3 shows the scattered photon spectrum at $E_\gamma = 16.58$ MeV for ^{52}Cr, Fe, ^{60}Ni, ^{92}Mo, and ^{96}Mo. These data are all "accepted" spectra, and the accidental coincidences have been subtracted. The peak near channel number 38 corresponds to nuclear elastic scattering, while a peak corresponding to inelastic scattering to the 2_1^+ level is indicated by an arrow. These spectra are essentially free of background, but a small tail due to multistep atomic processes in the target is evident in lower channels. In order to obtain the total number of counts in the elastic and inelastic peaks, a least-squares minimization procedure was used to fit the data to a sum of NaI response functions plus a simple parametrization of the background. The positions of the elastic and inelastic peaks were constrained by the energy calibration obtained with the detector placed directly in the incident photon beam and by the known excitation energies of excited states. Furthermore, since the NaI response functions were measured, the decomposition of the spectra into elastic and inelastic components could be done reliably and accurately. The results of one such fit are shown as the solid lines in Fig. 3. The cross sections deduced from this procedure were found to be relatively insensitive to the details of the background parametrization.

The relation between the number of scattered photons N_s detected in the NaI spectrometer and the differential cross section $d\sigma/d\Omega$ is

$$N_s = \kappa \frac{d\sigma}{d\Omega} \Omega_D N_\gamma \epsilon_s \tag{1}$$

where κ is the effective number of scattering centers per unit area (corrected by typically 15% for electronic interactions of the photons), Ω_D is the solid angle subtended by the detector, ϵ_s is the detector efficiency, and N_γ is the total number of tagged photons incident on the target. N_γ is proportional to the number of electrons N_{es} counted in the appropriate electron detector, and the proportionality constant is measured in the calibration procedure with the NaI directly in the incident photon beam:

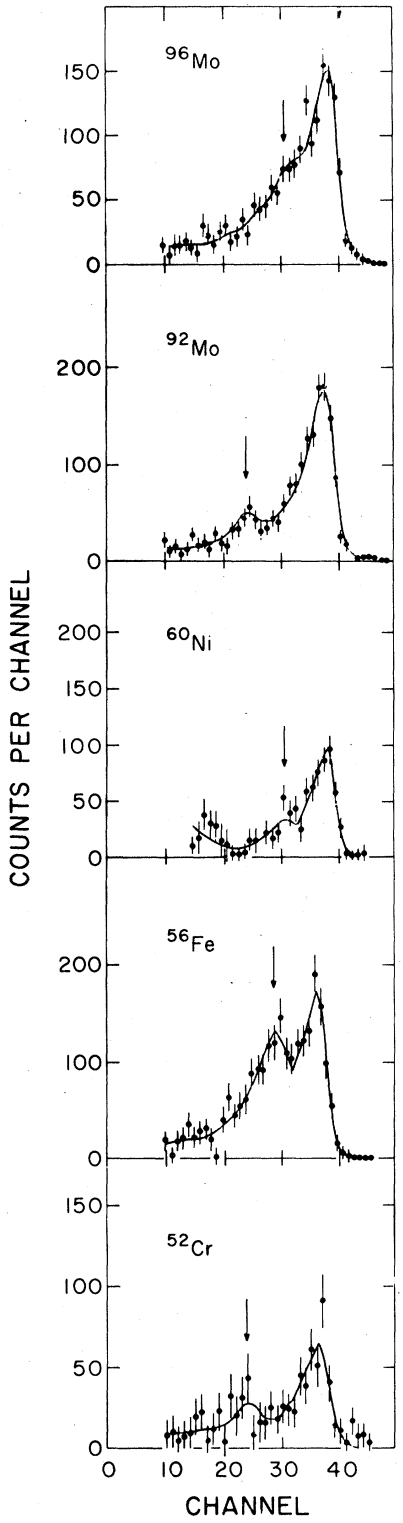

FIG. 3. Representative photon scattering spectra taken at $E_\gamma = 16.58$ MeV. The energy dispersion is 0.11 MeV/channel and channel 0 corresponds to 12.4 MeV. The peak near channel 38 corresponds to nuclear elastic scattering. The arrow indicates the expected position of a peak corresponding to inelastic scattering to the first excited state. The solid line is a fit to a sum of elastic and inelastic components plus a parametrized background, as discussed in the text.

$$N_\gamma = N_c N_{es} K / (N_{ec} \epsilon_c) \, . \tag{2}$$

For the calibration experiment, N_c/N_{ec} is the number of photons detected per tagging electron, ϵ_c is the detector efficiency, and K is a small correction factor due to the fact that the photon flux intercepted by the target is slightly different from that intercepted by the detector when it is in the photon beam. Thus

$$\frac{d\sigma}{d\Omega} = \frac{1}{\kappa} \frac{N_s/N_{es}}{N_c/N_{ec}} G \, , \tag{3}$$

where $G = [\Omega K \epsilon_s / \epsilon_c]^{-1}$. This expresses the cross section as the product of measurable quantities and a geometrical factor G. Note that to lowest order the detector efficiency need not be known absolutely, since the experimental geometry was chosen so that $\epsilon_s/\epsilon_c \approx 1$.

The value of G was determined in two independent ways. First, it was calculated using previously measured parametrizations of the photon beam profile to determine K. Second, it was empirically determined by scattering from the strong 15.1 MeV 1^+ level[16] in ^{12}C. One subtlety that arises in the measurement is that since this level is very narrow ($\Gamma < 40$ eV) compared with the width of the tagging counters ($\Delta E \sim 0.2$ MeV), the energy averaged cross section $\bar{\sigma}$ is sensitive to the precise value of ΔE:

$$\bar{\sigma} \equiv \frac{\int \sigma(E) dE}{\Delta E} = \frac{1.642 \text{ MeV mb}}{\Delta E} \, . \tag{4}$$

The numerator of this expression is taken from Ref. 16, and the quantity ΔE has been previously measured for the existing tagging counters. Thus an independent determination of G is possible. The two methods agree to within 20%. We adopt the mean for establishing the cross section scale, with an overall systematic uncertainty estimated to be $\pm 15\%$. The resulting cross sections are shown in Figs. 4–8. The error bars indicate statistical uncertainties only, and all data have been corrected for background. The inelastic cross section includes scattering to the 2_1^+ state only, and we estimate the cross section to the second excited state to be less than 25% of the 2_1^+ cross section.

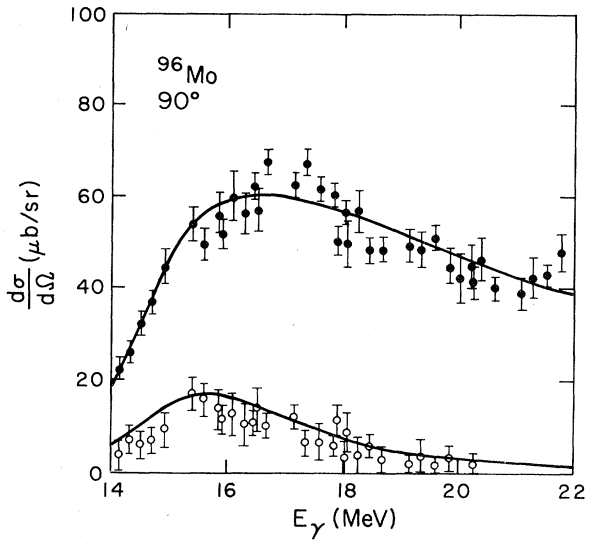

FIG. 4. Elastic (closed circles) and inelastic (open circles) scattering cross sections at $\theta=90°$ on ^{96}Mo. The error bars represent statistical uncertainties only. The solid lines are the DCM calculations for the elastic and inelastic cross sections. The curves corresponding to calculations with and without isospin splitting are indistinguishable.

In order to compare the present results with previous work, we have computed the elastic scattering cross section expected from the total photoabsorption cross section σ_γ, based on application of the optical theorem, a forward dispersion relation, and the dipole angular distribution. In these calculations, the Thompson scattering from the nuclear charge distribution was also included. σ_γ was taken from published (γ,Sn) results[17–19] for ^{92}Mo,

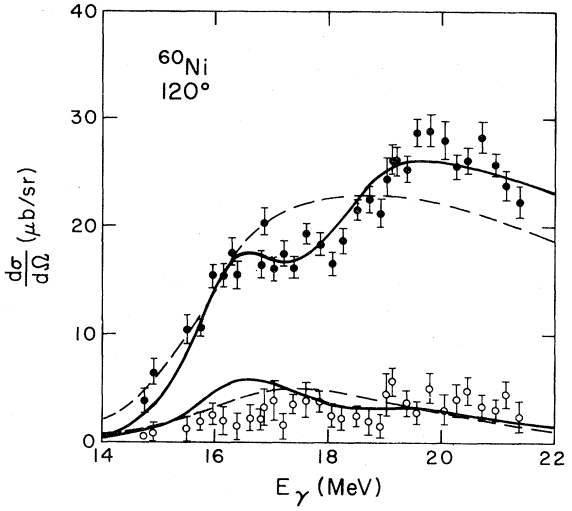

FIG. 6. Elastic (closed circles) and inelastic (open circles) scattering cross sections at $\theta=120°$ for ^{60}Ni. The error bars represent statistical uncertainties only. The solid (dashed) lines are DCM calculations for the elastic and inelastic cross sections including (not including) the effect of isospin splitting.

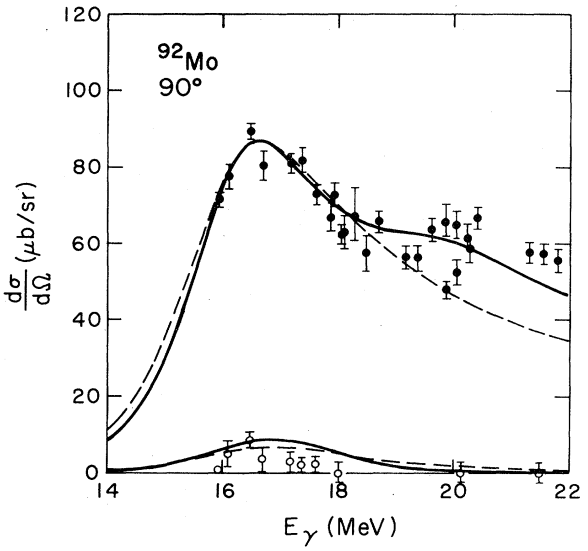

FIG. 5. Elastic (closed circles) and inelastic (open circles) scattering cross sections at $\theta=90°$ on ^{92}Mo. The error bars represent statistical uncertainties only. The solid (dashed) lines are DCM calculations for the elastic and inelastic cross sections including (not including) the effect of isospin splitting.

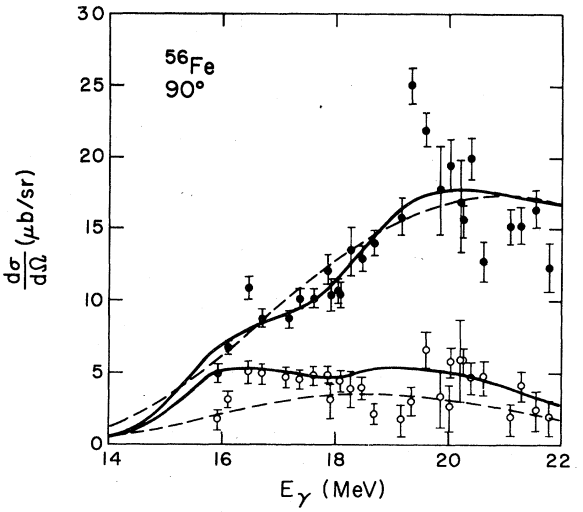

FIG. 7. Elastic (closed circles) and inelastic (open circles) scattering cross sections at $\theta=90°$ for ^{56}Fe. The error bars represent statistical uncertainties only. The solid (dashed) lines are DCM calculations for the elastic and inelastic cross sections including (not including) the effect of isospin splitting.

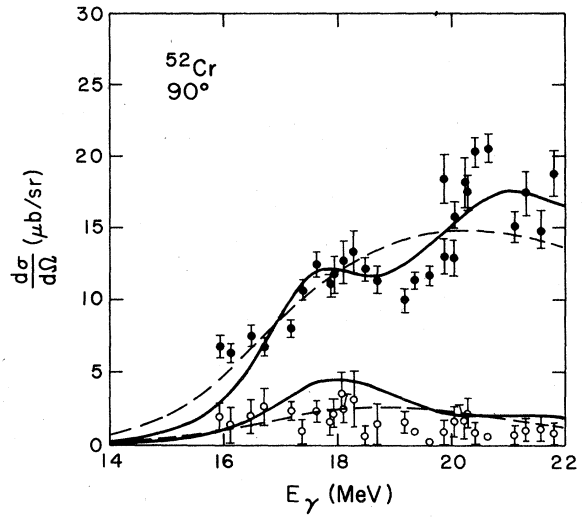

FIG. 8. Elastic (closed circles) and inelastic (open circles) scattering cross sections at $\theta=90°$ for ^{52}Cr. The error bars represent statistical uncertainties only. The solid (dashed) lines are DCM calculations for the elastic and inelastic cross sections including (not including) the effect of isospin splitting.

^{96}Mo, and ^{60}Ni plus (γ,Sp) results[19,20] for ^{92}Mo and ^{60}Ni. For ^{96}Mo, no (γ,Sp) data are available, but this cross section is not expected to be large.[17] For ^{52}Cr and ^{56}Fe, no σ_γ results are available. In order to see the effect of an uncertainty in the σ_γ normalization, scattering cross sections were computed for ^{96}Mo with a $\pm 10\%$ scale change and for ^{92}Mo and ^{60}Ni with a $\pm 15\%$ scale change in σ_γ. The comparison between these calculated cross sections and the present elastic scattering data is given in Fig. 9. These figures indicate that the present cross sections, even after allowing for a $\pm 15\%$ uncertainty in normalization, are generally lower (except for ^{60}Ni) than the lower limit allowed by previous results. Another possible concern for the analysis to follow is in the energy dependence of the cross sections. However, in view of the technique used in the scattering experiments, we believe that the relative accuracy of the present data is such that we can rule out the large fluctuations predicted for ^{60}Ni and the detailed shapes predicted for ^{92,96}Mo. The discrepancy is probably due to spurious structure in the measured (γ,p) cross sections and the lack of reliable (γ,p) data, since present-day techniques for the measurement of these cross sections are not as accurate as those used in (γ,n) or (γ,γ) measurements. Indeed the fluctuations predicted for ^{60}Ni and ^{92}Mo disappear

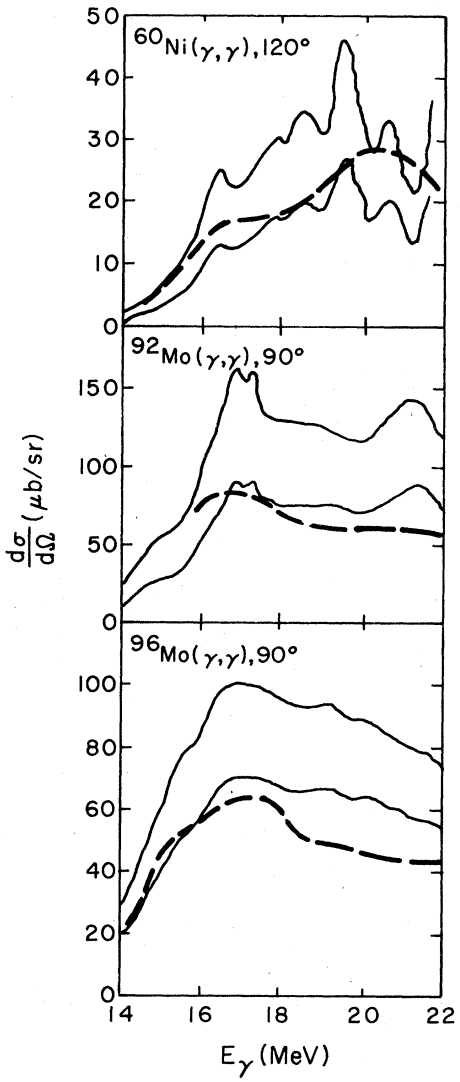

FIG. 9. Comparisons between the present elastic scattering data (dashed line) and calculations based on application of the optical theorem, a dispersion relation, and the dipole angular distribution to the photoabsorption cross section σ_γ, as discussed in the text. The solid lines represent the band of calculated cross sections with a $\pm 15\%$ error band on σ_γ for ^{92}Mo and ^{60}Ni and a $\pm 10\%$ error band on σ_γ for ^{96}Mo. There is a $\pm 15\%$ uncertainty in the normalization of the scattering data.

when the (γ,Sn) results alone are used for σ_γ. In summary, although there tends to be some disagreement between elastic scattering cross sections and the photoabsorption data, we believe the energy dependence as well as the relative amounts of elastic and inelastic scattering are of sufficient accuracy to test the DCM.

III. ANALYSIS IN TERMS OF DIPOLE-QUADRUPOLE COUPLING

A. Introduction

In the framework of the hydrodynamic model, the coupling between the giant dipole mode and surface degrees of freedom is a natural consequence of the boundary condition which requires that the outward flux of nuclear matter vanish at the surface.[21] This model accounts for the empirical fact that the energy of the GDR is proportional to R^{-1} (or equivalently to $A^{-1/3}$), where R is the nuclear radius. For permanently deformed, axially symmetric nuclei, it accounts for the splitting of the GDR into two modes corresponding to vibrations along ($K=0$) and perpendicular to ($K=1$) the symmetry axis.[22]

In spherical vibrational nuclei, the surface is dynamically deformed, which results in a modulation of the giant dipole vibration by the lower-frequency quadrupole surface vibrations. Bohr and Mottelson[3] characterize the strength of this coupling by the dimensionless parameter $\eta = \langle H_{DQ} \rangle / E_2$, where H_{DQ} is the dipole-quadrupole coupling energy and E_2 is the characteristic energy associated with a surface vibration. Since the dipole energy $E_1 \propto R^{-1}$, then $\langle H_{DQ} \rangle \sim kE_1\beta_0$, where β_0 is the zero-point vibrational amplitude and is related to the $E2$ transition rate connecting the ground state to the one-phonon first excited state by[23]

$$B(E2; 0^+ \rightarrow 2_1^+) = \left(\frac{3}{4\pi} Z R_0^2\right)^2 \beta_0^2 . \quad (5)$$

In the hydrodynamic model,[3] $k=0.76$, so that

$$\eta = 0.76 \frac{E_1 \beta_0}{E_2} . \quad (6)$$

In many cases η is of order 1 or greater (see, for example, Table I for the nuclei currently under study), thus implying a substantial coupling strength.

The approach of the DCM is to decompose the collective nuclear Hamiltonian into three terms: $H = H_Q + H_D + H_{DQ}$, where H_Q describes the low-lying quadrupole surface vibrations, H_D describes the uncoupled dipole mode, and H_{DQ} is the coupling term. The technique[4,24] is to diagonalize H in the basis of uncoupled solutions $|N_2,N_1\rangle$, where $N_2(N_1)$ is the number of quadrupole (dipole) phonons. In the absence of H_{DQ}, each low-lying quadrupole state $|N_2,0\rangle$ has a giant dipole excitation $|N_2,1\rangle$ built upon it, and all of the dipole photoabsorption cross section from the ground state $|0,0\rangle$ is concentrated in the lowest dipole state $|0,1\rangle$. Since H_{DQ} is essentially first order in the quadrupole vibrational amplitude, the surface vibrations become anharmonic whenever a dipole phonon is excited. Consequently dipole states with different N_2 mix. Since the $|0,1\rangle$ component mixes into several physical dipole states, the photoabsorption strength spreads in energy over an interval of order $\eta E_2 \approx \beta_0 E_1$.[3] Indeed, most of the evidence supporting the DCM comes from the systematic variation of the width of the GDR with β_0.[4] Furthermore, since photon scattering is a two-step process of absorption followed by reemission, then inelastic photon scattering probes the vibrational composition of the dipole states. For example, the inelastic scattering amplitude through a particular intermediate dipole state to the $|N_2,0\rangle$ level is proportional to the product of the $|0,1\rangle$ and $|N_2,1\rangle$ amplitudes in that intermediate state, and this scattering amplitude should scale roughly with η.[5]

TABLE I. Parameters used in the DCM calculations without isospin splitting.

Nucleus	E_1[a] (MeV)	E_2 (MeV)	β_0	η[b]	Γ_0[a] (MeV)	δ[a]	S[a]
^{96}Mo	16.25	0.778	0.18	2.9	4.4	4.6	0.92
^{92}Mo	16.32	1.508	0.10	0.8	3.4	2.9	0.70
^{60}Ni	17.94	1.332	0.21	2.2	4.0	1.5	0.60
^{56}Fe	18.00	0.847	0.25	4.0	5.2	0	0.78
^{52}Cr	18.15	1.434	0.20	1.9	5.0	0	0.69

[a]Determined from a least-squares fit to the elastic data.
[b]Calculated from Eq. (6).

B. Description of the DCM calculations

For the present calculations, we have utilized the computer code AREZ,[25] in which H_Q is treated in the *harmonic approximation* and is therefore completely specified by the parameters E_2 and β_0. The appropriateness of this assumption will be discussed in Sec. IV. H_D requires only the unperturbed dipole energy E_1, which in the strict hydrodynamic model is equal to $80A^{-1/3}$ MeV.[21] However, we have allowed E_1 to vary in order to provide the best overlap (in the least-squares sense) with the elastic scattering data. Both H_{DQ} and the dipole operator D were treated in the hydrodynamic model and included terms up to second order in the surface vibrational amplitude. The coupling constants were taken from Rezwani *et al.*,[24] and the zeroth order dipole operator was scaled so that the total integrated photoabsorption cross section corresponds to one classical dipole sum rule.

The energy matrix was diagonalized in a space including up to 15 surface phonons corresponding to 72 different dipole states $|N\rangle$. For each of these the energies, E_N, and the dipole matrix elements connecting to vibrational states $|f\rangle$, $\langle N||D||f\rangle$, were calculated. These quantities are related to the scattering cross sections as follows[24]:

$$\frac{d\sigma}{d\Omega}\bigg|_{0\to f}(E,\theta)=\frac{E'}{E}\left[\frac{(1+\cos^2\theta)}{6}|P_0|^2+\frac{(13+\cos^2\theta)}{12}|P_2|^2\right], \tag{7}$$

where the scalar (tensor) polarizability $P_0(P_2)$ is given by

$$P_j=\delta_{jI_f}[3(2I_f+1)]^{-1/2}\frac{EE'}{(\hbar c)^2}\sum_{N=1}^{72}\langle f||D||N\rangle\langle N||D||0\rangle \times\left[\left[E_N+E'+\frac{i\Gamma_N}{2}\right]^{-1}+\left[E_N-E-\frac{i\Gamma_N}{2}\right]^{-1}\right]-\delta_{j0}\delta_{0f}\frac{\sqrt{3}(Ze)^2}{AMc^2}. \tag{8}$$

In these expressions, $E(E')$ is the energy of the incident (scattered) photon. We have implicitly assumed that the initial state $|0\rangle$ and final state $|f\rangle$ have $J^\pi=0^+$ and $I_f{}^+$, respectively, and that the photons are unpolarized. Therefore j corresponds to the angular momentum transferred to the nucleus in the scattering process, so that only the scalar term contributes to elastic scattering and only the tensor term contributes to inelastic scattering to a 2^+ state. Furthermore, the last term in Eq. (8) is the Thompson amplitude, which contributes coherently to the elastic process. Other possible non-nuclear contributions to elastic scattering (e.g., Rayleigh and Delbrück) are not expected to be important[26] and are not included.

Since all the dipole states contribute coherently to the scattering process, the scattering cross section is very sensitive to the relative degree of overlap among these states. Thus the damping widths, Γ_N, of the various levels are important parameters in determining the scattering cross sections, although they are the parameters least well determined by theory. The DCM itself does not predict these widths. In order to provide a meaningful comparison between the calculations and the data, we have parametrized the Γ_N according to the prescription of Danos and Greiner,[27]

$$\Gamma_N=\Gamma_0(E_N/E_1)^\delta, \tag{9}$$

and determined Γ_0 and δ by a least-squares fit of Eqs. (7) and (8) to the elastic scattering data. This is a more sensitive constraint on the value of Γ_N than a fit to total photoabsorption data, since in the latter process the different dipole states contribute incoherently. The unperturbed dipole energy E_1 was also allowed to vary in the fit, as discussed above. Finally we have multiplied the calculated cross sections (both elastic and inelastic) by an overall scale factor S, which we also allowed to vary in the fit. Thus we are not testing the DCM for its ability to predict absolute cross sections in order that we avoid questions concerning the fraction of sum rule strength contained in the GDR and the accuracy of the experimental cross section scale (see Sec. II). The ratio between the experimental cross sections and the cross sections expected on the basis of 1 classical dipole sum rule is represented by S. Once the scale factor S and the parameters E_1, Γ_0, and δ are determined, the ine-

lastic cross section can be calculated and compared directly with the data.

C. Isospin splitting of the GDR

One of the assumptions of the DCM is that there is a single unperturbed dipole state which splits into several vibrational satellites. However, since the GDR is an isovector excitation, the dipole strength in nuclei with a neutron excess ($T \equiv (N-Z)/2 > 0$) is shared between a $T_< \equiv T$ and a $T_> \equiv T+1$ component,[7] and these components are split in energy primarily by the nuclear symmetry potential.[7] Since this splitting is of the same order of magnitude as the splitting due to the coupling to surface vibrations, a proper description of the GDR would treat the two effects in a self-consistent manner. Such a description is beyond the scope of present theories, since isospin is not an inherent ingredient of the DCM. Nevertheless, in order to provide a meaningful comparison with the scattering data, it was necessary to include the effects of isospin splitting, as we shall show below. Therefore, we have incorporated isospin splitting into the DCM in an *ad hoc* manner. We start with 2 unperturbed dipole states (the $T_<$- and $T_>$-states) which are split in energy by an amount[7]

$$\Delta E \equiv E_> - E_< = 60(T+1)/A \text{ MeV} \qquad (10)$$

and have integrated photoabsorption strengths in the ratio[7]

$$R \equiv \frac{\int \sigma_> dE}{\int \sigma_< dE} = \frac{E_>}{E_< T}\left|\frac{1-1.5(TA^{-2/3})}{1+1.5A^{-2/3}-4T(T+1)A^{-2}}\right| . \qquad (11)$$

Note that as the neutron excess gets larger, the dipole strength becomes more concentrated in the $T_<$- component. The DCM acts on each component separately and generates a set of 144 dipole states (72 for each isospin). At this point all reference to isospin is dropped and all states are thereafter treated on an equal footing in the computation of dipole matrix elements and scattering cross sections. As described above, the parameters $E_1 (\equiv E_<)$, Γ_0, δ, and S were determined by fitting to the elastic data. ΔE and R were not fitted parameters but were constrained by Eqs. (10) and (11).

D. Comparison with the scattering data

In Figs. 4–8, the calculated cross sections are superimposed upon the data. The solid (dashed) lines are the cross sections calculated with (without) isospin splitting, and the relevant parameters are given in Table I (II). The DCM results for the distribution of ground-state dipole strength are presented in Fig. 10 (isospin splitting included). We now discuss in more detail the qualitative features of the calculations and the data for each of the nuclei studied.

^{92}Mo ($T=4$).

Since $\eta \approx 0.8$, one expects relatively weak coupling between dipole and surface modes. This is evident in both the calculations and the data in which the apparent splitting of the dipole strength and the ratio of inelastic to elastic scattering are small. In fact, the calculations show [Fig. 10(b)] that for each isospin component, the dipole strength is concentrated in one dominant state which is located just below E_1, and one weaker sa-

TABLE II. Parameters used in the DCM calculations including isospin splitting. The quantities β_0 and E_2 are the same as in Table I and η is given by Eq. (6).

Nucleus	T	R[a]	E_1[b] (MeV)	ΔE[c] (MeV)	Γ_0[b] (MeV)	δ[b]	S[b]
^{96}Mo	6	0.11	16.15	4.38	3.6	3.20	0.83
^{92}Mo	4	0.20	16.43	3.26	3.0	0.77	0.77
^{60}Ni	2	0.43	17.37	3.00	2.6	1.28	0.49
^{56}Fe	2	0.43	17.69	3.21	2.4	0	0.53
^{52}Cr	2	0.43	18.54	3.46	2.8	0.49	0.61

[a]Calculated from Eq. (11).
[b]Determined from a least-squares fit to the elastic data.
[c]Calculated from Eq. (10).

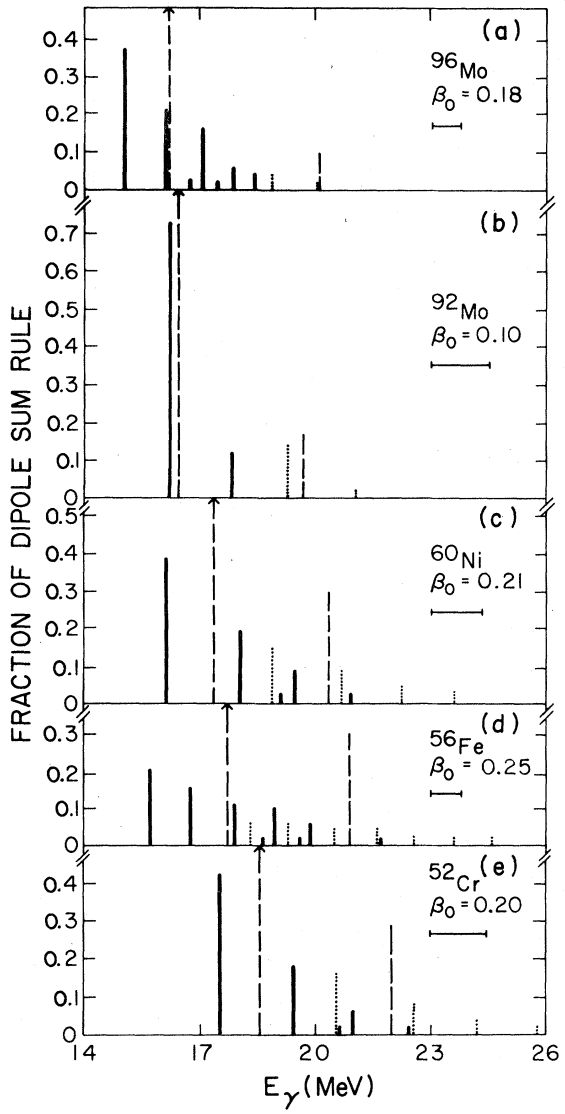

FIG. 10. Distribution of $E1$ strength calculated using the DCM with isospin splitting. The dashed lines indicate the positions and relative strengths of the unperturbed $T_<$ and $T_>$ states. The solid bars (dots) show the calculated position and strength of the $T_<$ ($T_>$) states. The vertical scale is such that 1.0 corresponds to 1 dipole sum rule. For reference, the excitation energy of the first excited state is indicated by the length of the horizontal bar.

tellite resonance which is located slightly above E_1+E_2. This is a classic case of weak coupling and explicit calculations show that two-level, first order perturbation theory does about as well as the full calculation. In Fig. 5, we see that inclusion of T splitting is necessary to explain the excess of scattering above 20 MeV and that once this is included, the elastic cross section is well accounted for by the DCM. The inelastic scattering is overpredicted by the DCM, but the gross energy dependence of the data seems to be reproduced by the calculation.

$^{96}Mo(T=6)$.

This nucleus offers an interesting contrast to ^{92}Mo since the coupling should be much larger ($\eta \approx 2.9$). Consequently one expects a greater splitting of the dipole strength and a significantly greater amount of inelastic scattering. Both the calculations and the data confirm this. The distribution of dipole strength [Fig. 10(a)] appears as a nearly harmonic sequence with spacing on the order of E_2, with the lowest state well below E_1 and with the dipole strengths monotonically decreasing with increasing energy. For each isospin about 5 dipole states carry significant strength. The agreement between the measured elastic and inelastic cross sections and the calculation is remarkable (Fig. 4), and the inclusion of T splitting has no appreciable effect on these cross sections ($R \approx 0.11$).

^{60}Ni and $^{52}Cr(T=2)$.

These nuclei have similar coupling to the surface ($\eta \approx 2.2$ and 1.9, respectively) and the distribution of dipole strength for each isospin looks similar to ^{96}Mo [Fig. 10(c), (e)] except that only 3—4 components have significant dipole strength. The calculations further show that without including T splitting, the DCM does not provide enough dipole strength above 20 MeV to account for the elastic scattering data. The only way the least-squares minimization routine can fit the data is to make Γ_0 unreasonably large so that the calculated curve goes through the gross average of the data. However, it is clear from Figs. 6 and 8 that the dashed curve does not adequately account for the structure in the elastic cross section, and the fact that the calculation agrees with the inelastic data must be considered fortuitous. The solid curve much better accounts for the elastic data, although discrepancies in the inelastic data are apparent. For example, in both nuclei the DCM overpredicts the inelastic cross section in the region of the $T_<$ resonance.

$^{56}Fe(T=2)$.

This nucleus has the largest coupling parameter ($\eta \approx 4.0$) of those studied and this is reflected both in the distribution of dipole strength [Fig. 10(d)]

and in the magnitude of the inelastic scattering (Fig. 7). For each isospin about 6 states have significant dipole strength, and, as in the other $T=2$ nuclei, isospin splitting is necessary to explain the elastic data. It also appears from Fig. 7 that the DCM with T splitting qualitatively accounts for the strength and energy dependence of the inelastic scattering. Finally we point out that the fine structure peak in the elastic data just below 20 MeV, which was confirmed in a subsequent experiment, is not accounted for by the DCM and may have a quite different origin.

IV. DISCUSSION

In this section we summarize the important conclusions to be drawn from the DCM analysis, emphasizing first the successes and then the failures of the model. First, the DCM succeeds in qualitatively accounting for the scaling of the inelastic scattering cross sections with the parameter η: In nuclei where η is large the scattering is large, and in nuclei where η is small, the scattering is small. In particular, the differences between ^{92}Mo and ^{96}Mo and the similarities between ^{52}Cr and ^{60}Ni represent qualitative successes for the model. For ^{96}Mo, the model does remarkably well quantitatively in describing both the elastic and the inelastic data. Also the calculations predict that inelastic scattering to higher-lying levels is considerably weaker than scattering to the 2_1^+ level, in agreement with the experimental observations. Finally, as already pointed out by Beil *et al.*,[17] the total width of the GDR in the $A\approx 90$ region scales in the expected manner with β_0.

Despite these qualitative successes, deficiencies in the DCM become apparent as we look at the lighter nuclei. We have seen that it is generally not possible for the DCM to account for the energy dependence of the elastic scattering without an additional mechanism for splitting the dipole strength. The isospin splitting of the GDR, although treated in an *ad hoc* manner, seems to improve the description of the elastic data. Far more serious discrepancies are apparent in the inelastic data. In each of the $T=2$ nuclei, the detailed energy dependence of the inelastic cross section is not reproduced by the calculation. For example, in ^{60}Ni too much inelastic scattering is predicted near the $T_<$ position and too little near the $T_>$ position. For ^{52}Cr, the predicted inelastic scattering is greater than the data nearly everywhere. Furthermore, in ^{92}Mo, the predicted magnitude of the inelastic cross section is $2-3$ times larger than the data. This latter discrepancy is particularly disturbing since the possible complication due to isospin splitting is expected to be less important than in the lighter nuclei. Furthermore, of the nuclei studied, ^{92}Mo has the weakest coupling ($\eta\approx 0.8$) and is the nucleus for which the harmonic approximation is most likely to be valid. Thus one would expect that ^{92}Mo is an ideal nucleus to test the DCM, yet it is the nucleus where the discrepancies in the inelastic cross sections are most severe. A similar discrepancy has recently been reported[28] in ^{166}Er, where the DCM overpredicts by a factor of $2-4$ the inelastic scattering cross section to the γ-vibrational band head. As in ^{92}Mo, this is particularly significant since the collective nature of the low-lying states in ^{166}Er is well understood. It is curious that the DCM works so poorly in ^{92}Mo and ^{166}Er and yet so well in ^{96}Mo, where the coupling is much stronger and the harmonic approximation is less likely to be valid. It seems clear that there is still much to be understood about the dynamics of the coupling of the GDR to other collective modes and that, despite its qualitative successes, the DCM does not provide an adequate description of this coupling. It may be that the DCM, which treats the coupled vibrations in macroscopic collective coordinates, is too crude and that a microscopic calculation in the framework of the random phase approximation will provide the refinement needed to describe the present data.

V. SUMMARY AND CONCLUSIONS

We have studied the photon-decay modes of the GDR in several medium-weight nuclei using the photon-scattering reaction. The elastic scattering data show clear evidence for the isospin splitting of the GDR, in reasonable agreement with the model of Fallieros *et al.*[7] We have attempted to interpret the inelastic scattering data in terms of the coupling between the GDR and surface vibrations. The rough scaling of the inelastic scattering cross section with the coupling parameter η suggests that our basic understanding of the reaction mechanism is correct. However, a particular model for this coupling, the dynamic collective model, fails to adequately account for the details of the inelastic cross sections.

We gratefully acknowledge the participation of Dr. Richard Starr in the early stages of this

research. The research carried out by the University of Illinois staff, including the development and operation of MUSL-2 and its experimental areas, was supported by the National Science Foundation. The research carried out by the Argonne staff was supported by the Department of Energy.

*Physics Division, Los Alamos Scientific Laboratory, Los Alamos, New Mexico 87545.
†Physics Department, California Institute of Technology, Pasadena, California 91125.

[1]A. Bohr and B. Mottelson, *Nuclear Structure* (Benjamin, Reading, Mass., 1975), Vol. II, p. 503 ff.
[2]J. J. Sakurai, *Advanced Quantum Mechanics* (Addison-Wesley, Reading, Mass., 1967), p. 57 ff.
[3]A. Bohr and B. Mottelson, *Nuclear Structure* (Benjamin, Reading, Mass., 1975), Vol. II, p. 453 ff.
[4]J. LeTourneux, K. Dan. Vidensk. Selsk. Mat. Fys. Medd. 34, 11 (1965); M. G. Huber, M. Danos, H. J. Weber, and W. Greiner, Phys. Rev. 155, 1073 (1967).
[5]H. Arenhövel and H. J. Weber, Nucl. Phys. A91, 145 (1967).
[6]M. Danos and W. Greiner, Phys. Rev. 134, B284 (1964).
[7]S. Fallieros and B. Goulard, Nucl. Phys. A147, 593 (1970); R. O. Akyüz and S. Fallieros, Phys. Rev. Lett. 27, 1016 (1971).
[8]T. J. Bowles, R. J. Holt, H. E. Jackson, R. M. Laszewski, A. M. Nathan, J. R. Specht, and R. Starr, Phys. Rev. Lett. 41, 1095 (1978).
[9]A. M. Nathan, R. M. Laszewski, T. J. Bowles, R. J. Holt, H. E. Jackson, and R. McKeown, Bull. Am. Phys. Soc. 24, 648 (1979).
[10]T. Bar-Noy and R. Moreh, Nucl. Phys. A275, 192 (1977).
[11]H. E. Jackson and K. J. Wetzel, Phys. Rev. Lett. 28, 513 (1972).
[12]E. Hayward, W. C. Barber, and J. Sazama, Phys. Rev. C 8, 1065 (1973); E. Hayward, W. C. Barber, and J. J. McCarthy, *ibid.* 10, 2652 (1974).
[13]H. Arenhövel and J. M. Maison, Nucl. Phys. A147, 305 (1970).
[14]J. S. O'Connell, P. A. Tipler, and P. Axel, Phys. Rev. 126, 228 (1962); R. M. Laszewski and P. Axel, *ibid.* 19, 342 (1979).
[15]M. D. Hasinoff, S. T. Lim, D. F. Measday, and T. J. Mulligan, Nucl. Instrum. Methods 117, 375 (1974).
[16]B. T. Chertok, C. Sneffield, J. W. Lightbody, S. Penner, and D. Blum, Phys. Rev. C 8, 23 (1973); H. W. Kuehne, P. Axel, and D. Sutton, Phys. Rev. 163, 1278 (1967).
[17]H. Beil, R. Bergère, P. Carlos, A. Leprêtre, A. DeMiniac, and A. Veyssière, Nucl. Phys. A227, 427 (1974).
[18]S. C. Fultz, R. A. Alvarez, B. L. Berman, and P. Meyer, Phys. Rev. C 10, 608 (1974).
[19]K. Shoda, Phys. Rep. 53, 341 (1979).
[20]H. Miyase, S. Oikawa, A. Suzuki, J. Uegaki, T. Saito, M. Sugawara, and K. Shoda, in *Proceedings of the International Conference on Photonuclear Reactions and Applications, Asilomar, 1973,* edited by B. L. Berman (USAEC Office of Information Services, Oak Ridge, 1973), p. 5B8-1.
[21]J. Eisenberg and W. Greiner, *Nuclear Models* (North-Holland, Amsterdam, 1970), Vol. I, p. 275 ff.
[22]M. Danos, Nucl. Phys. 5, 23 (1958); K. Okamoto, Phys. Rev. 110, 143 (1958).
[23]A. Bohr and B. Mottleson, *Nuclear Structure* (Benjamin, Reading, Mass., 1975), Vol. II, p. 349.
[24]V. Rezwani, G. Gneuss, and H. Arenhövel, Nucl. Phys. A180, 254 (1972).
[25]H. Arenhövel, private communication.
[26]R. Moreh, in *Lecture Notes in Physics,* edited by H. Arenhövel and D. Drechsel (Springer, Berlin, 1979), Vol. 108, p. 276 ff.
[27]M. Danos and W. Greiner, Phys. Rev. 138, B876 (1965).
[28]A. M. Nathan and R. Moreh, Phys. Lett. 91B, 38 (1980).